UNIVERSITAT DE BARCELONA

Departament d'Astronomia i Meteorologia

Astrophysical Studies on Open Clusters:

NGC 1807, NGC 1817, NGC 2548 and NGC 2682

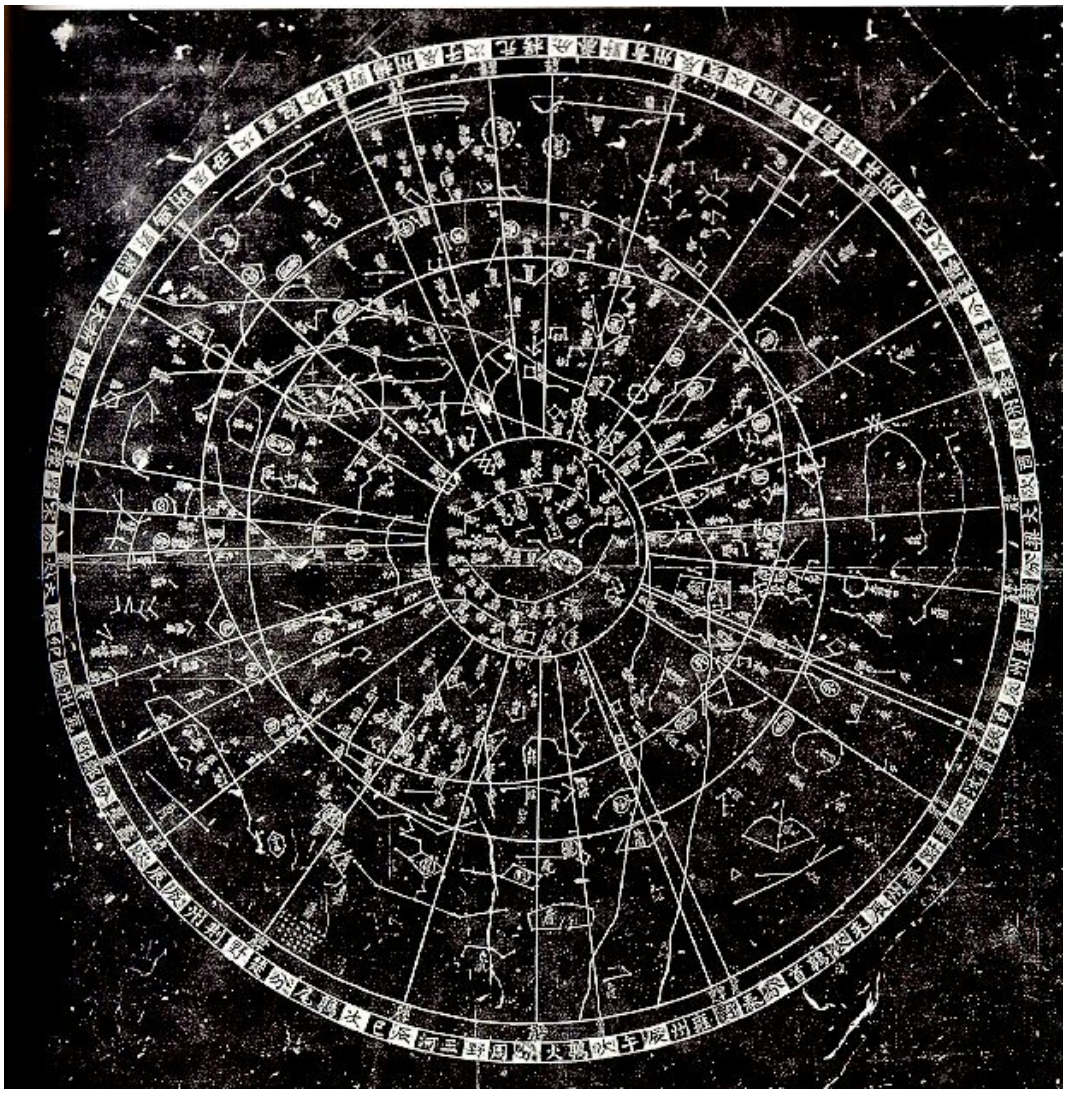

Memoria presentada por

María de los Dolores Balaguer Núñez

para optar al grado de

Doctora en Física

Barcelona, 31 de octubre de 2005

旅夜書懷

細草微風岸，危檣獨夜舟。
星垂平野闊，月湧大江流。
名豈文章著，官應老病休。
飄飄何所似，天地一沙鷗。

杜甫 (712-770)

A night abroad

A light wind is rippling at the grassy shore...
Through the night, to my motionless tall mast,
The stars lean down from open space,
And the moon comes running up the river.
...If only my art might bring me fame
And free my sick old age from office!–
Flitting, flitting, what am I like
But a sand-snipe in the wide, wide world!

Du Fu (712 - 770)

6 NGC 2682 (M 67): $uvby - H_\beta$ CCD Photometry and membership segregation

Photometric studies of NGC 2682 (M 67) have been performed by several authors. Montgomery et al. (1993) have presented a deep ($V \sim 20$) $UBVI$ CCD photometry of 1468 stars within 15′ of the centre of the cluster, and Fan et al. (1996) have studied spectrophotometry of similar depth in nine BATC intermediate-band filters for stars in a 1.°92 × 1.°92 area centred on the cluster. In addition, variability studies have been performed in M 67, most notably by Gilliland et al. (1993), who conducted a very sensitive, highly temporally sampled study of stars in the central few arcmin of the cluster. Stassun et al. (2002) using differential CCD photometry to search for variability, obtained sensitive photometry of 990 stars in a roughly square region one-third of a degree on a side centred 5′ north of the cluster centre. Sandquist (2004) also as a by-product of variability studies, conducted a relative high precision VI colour-magnitude diagram analysis.

Nissen et al. (1987) obtained accurate $uvby - H_\beta$ photoelectric photometry of a sample of 79 stars in a radius of 10′ from the centre, from subgiant branch down to the unevolved main sequence. For this reason stars in M 67 were used by us as photometric standard stars for the observations of NGC 1817 and NGC 2548 (Chapters 3 and 5). The amount of observations taken allowed us to obtain high quality photometry of this cluster. In spite of being a very well studied cluster, our Strömgren photometry deserves an analysis both because of the deepness and extension covered.

There are also a number of proper motion and radial velocity studies. Sanders

(1977) calculated probabilities of membership based on relative proper motions of 1866 stars in the cluster field with a limiting photographic magnitude of approximately 17. From 10 plate pairs of different origin and with a maximum epoch difference of 68 years, he finds 649 probable members. Girard et al. (1989) gave relative proper motions for 663 stars in an area of $42' \times 34'$ from 44 plates with a maximum separation of 66 years. Although the plates used were of different depths, the deepest plates provided a limiting visual magnitude down to 16. In 1993, Zhao et al. derived relative proper motions of 1046 stars within a $1\overset{\circ}{.}5 \times 1\overset{\circ}{.}5$ area in the region from PDS measurements of 9 plates with a maximum epoch difference of 80 years and a magnitude limit $V \sim 15.5$.

On the other hand, the radial velocity studies by Mathieu et al. (1986, 1990) gave precise radial-velocity measurements for 170 stars, including all main-sequence stars brighter than $V = 12.8$.

In this Chapter we discuss the results of our CCD photometric study of NGC 2682, covering an area of about $50' \times 50'$ (Figure 6.1) down to $V \sim 19$, and a new membership segregation based on the comparison between parametric and non-parametric methods applied to the above-mentioned proper motions from Zhao et al. (1993). This study was selected among all other existent because it covers the biggest area and largest epoch difference. Also, this material is fully homogeneous with that used for the other clusters in this work, as from the point of view of telescope and plates, as from the point of view of proper motion treatment and reduction. We followed the same process to derive the physical parameters already used in previous Chapters.

6.1 The Data

6.1.1 Observations

The Strömgren CCD photometry of the area was obtained at the same observatories and nights as explained at length in Chapters 3 and 5, because the stars of NGC 2682 with known photometry were used to transform instrumental magnitudes to the standard system. We have observations from CAHA, OAN and WFC-INT, as in previous Chapters, however due to the quality and the wide area coverage of the

Table 6.1: Log of the observations used

Telescope	Date	Seeing(″)	n. of frames	Exp. Times (s)				
				u	v	b	y	H_β
1.23 m CAHA	2000/01/05-10	1.1	20					90
1 m JKT	2000/02/02-06	1.1	42	-	-	-	-	200
2.5 m WFC-INT	2000/02/02-03	1.3	44	80	20	20	10	-

WFC-INT images, we only use those in the analysis for u, v, b, y filters. For the H_β filters, not available in the WFC, we used the JKT and CAHA observations. A log of the observations, the total number of frames, exposure times and seeing conditions is given in Table 6.1.

As the standard stars are mostly located in the central area of the cluster, the telescope was pointed to several positions in the cluster region to make the centre of the cluster fall on the four different chips of the WFC mosaic making feasible the calibration for all four chips. Thus the area covered is larger than in any previous studies of this cluster in the Strömgren system.

We obtained photometry for a total of 1843 stars in an area of $50' \times 50'$ in NGC 2682 region, down to a limiting magnitude $V \sim 19$. The area covered is shown in the finding chart of the cluster (Figure 6.1). Since the H_β measurements were only taken at the JKT and CAHA telescopes, the spatial coverage with this filter is limited. Only 288 stars (placed in the central region) have H_β values.

6.1.2 Reduction and transformation to standard system

The reduction of the photometry is explained at length in Chapter 3. We performed the transformation to the standard system using the same procedures as in the other clusters (Sections 3.1.2 and 5.1.2). Due to the fact of having the standard stars in the same images, the process is, in this case, equivalent to having performed differential photometry.

The coefficients of the transformation equations were computed by a least squares method using the instrumental magnitudes of the standard stars and the standard

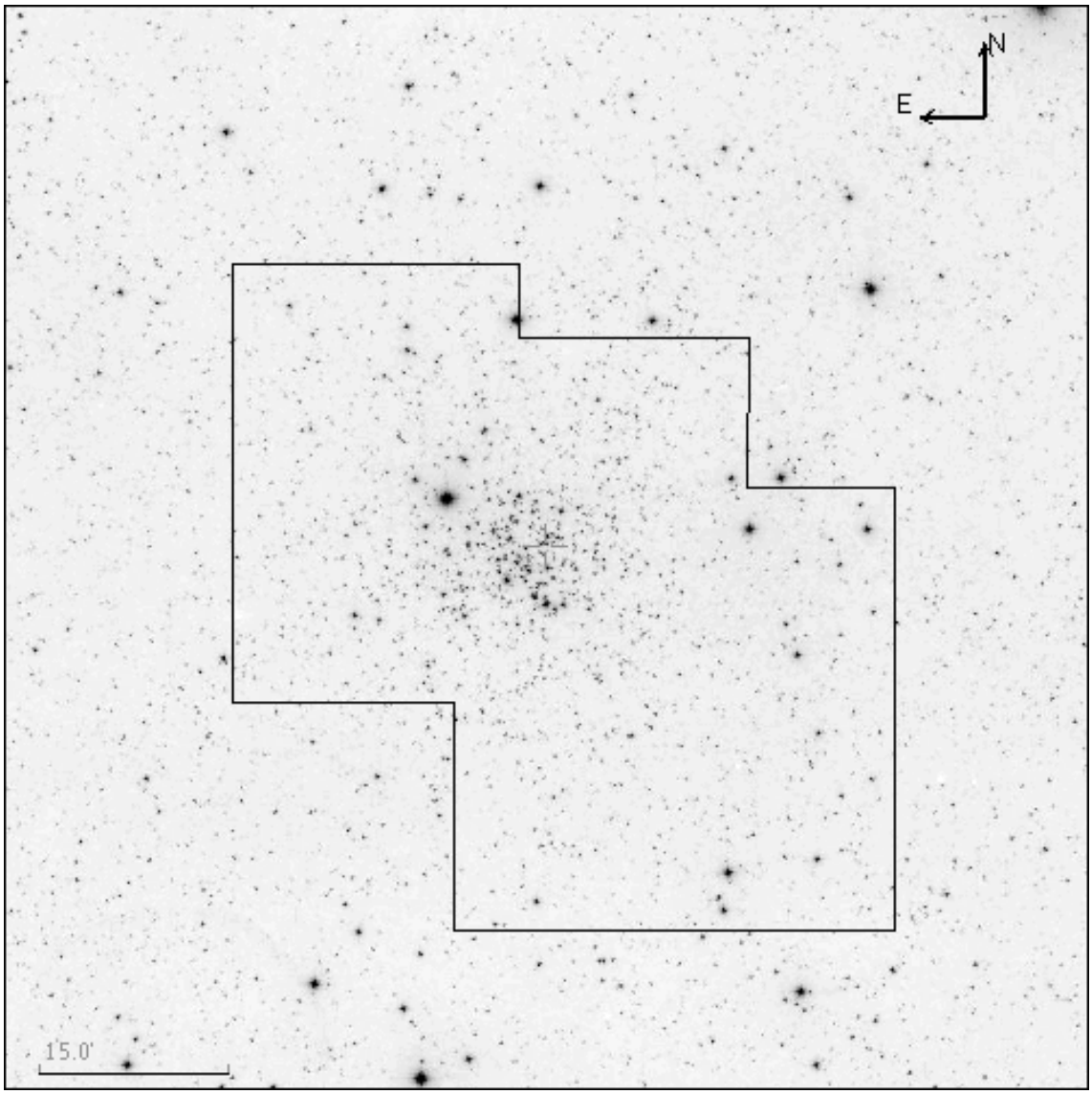

Figure 6.1: Finding chart of the area under study. The covered area is marked in black on an image of a plate (POSSI.E—optical R—.DSS1.486-LOW) plotted with Aladin (Bonnarel et al. 2000).

Table 6.2: Number of observed stars (N) and mean internal errors (σ) as a function of apparent visual magnitude.

V range	V		$(b-y)$		m_1		c_1		H_β	
	N	σ	N	σ	N	σ	N	σ	N	σ
8- 9	3	0.029	3	0.028	3	0.029	2	0.004		
9-10	8	0.008	7	0.007	6	0.008	7	0.007	2	0.001
10-11	22	0.003	22	0.002	22	0.003	22	0.005	10	0.009
11-12	28	0.004	28	0.022	26	0.003	26	0.005	14	0.016
12-13	114	0.004	114	0.003	114	0.004	114	0.005	56	0.009
13-14	199	0.003	199	0.003	198	0.004	197	0.006	75	0.015
14-15	240	0.020	239	0.005	238	0.006	237	0.009	63	0.016
15-16	277	0.007	277	0.010	275	0.011	269	0.018	57	0.019
16-17	299	0.011	299	0.015	272	0.021	233	0.031	10	0.016
17-18	307	0.021	306	0.029	245	0.041	109	0.043	1	0.033
18-19	259	0.040	259	0.058	130	0.073	46	0.059		
19-20	75	0.093	75	0.125	18	0.141	12	0.106		
Total	1831		1828		1547		1274		288	

magnitudes and colours in the $uvby - H_\beta$ system. Up to 68 stars in the field of the cluster have known photometry from Nissen et al. (1987) and they were considered standard stars. Ten short exposures in each filter were taken every night with a magnitude limit of $V \sim 19$. At least one exposure per filter was pointed to make the centre of the cluster fall on each of the WFC chips. Those standard stars with residuals greater than 2σ were rejected. As in the previous clusters, the reduction was performed for each night independently and in two steps, following the Equations (3.1) to (3.6).

The final errors as a function of apparent visual magnitude are given in Table 6.2 and plotted in Figure 6.2.

Table 6.3[2] lists the u, v, b, y, H_β data for all 1843 stars in a region of $50' \times 50'$ around the open cluster NGC 2682 (Figure 6.1). Star centres are given as frame (x, y) and equatorial ($\alpha_{\rm J2000}$,$\delta_{\rm J2000}$) coordinates. An identification number was assigned to every star following the order of increasing right ascension. Column 1 is the ordinal

[2]Table 6.3 is available in electronic form from `Lola.Balaguer@am.ub.es`.

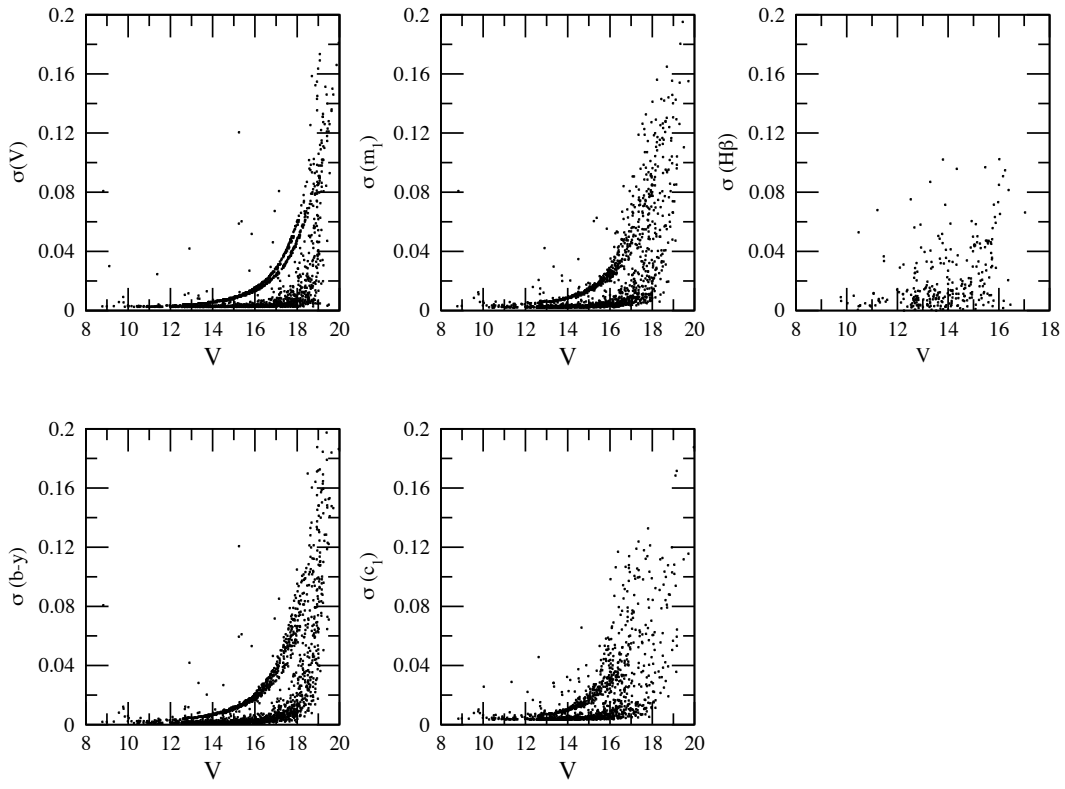

Figure 6.2: Mean internal errors of magnitude and colours as a function of the apparent visual magnitude, V, for all observed stars in the cluster region.The structure in the magnitude dependence is mainly owed to different numbers of measurements for individual stars since the center of the cluster was shifted to be observed by each of the four CCD chips.

star number; columns 2 and 3 are α_{J2000} and δ_{J2000}; columns 4 and 5 are the respective x, y coordinates in arcmin; columns 6 and 7 are the $(b-y)$ and its error, 8 and 9 the V magnitude and its error, 10 and 11 the m_1 and its error, 12 and 13 the c_1 and its error, and 14 and 15 the H_β and its error. In column 16, stars considered candidate members (see Section 6.3.1) are labelled 'M', while those classified as non-members show the label 'NM'.

The cross-identification of stars in common with the astrometry (Zhao et al. 1993), BDA (`http://obswww.unige.ch/WEBDA`), Hipparcos (ESA, 1997), Tycho-2 (Høg et al. 2000) and USNO-2 (Monet et al. 1998) catalogues is provided in Table 6.4[3].

6.1.3 Comparison with previous photometry

After Nissen et al. (1987), few studies have been done in Strömgren photometry. Anthony-Twarog (1987) used a CCD to cover an area bigger than Nissen's, with up to 44 stars in common with our work sample. Comparing Anthony-Twarog's data with ours, the mean differences in the sense ours minus others, we get $-0.01(\sigma = 0.04)$ in V, 0.00(0.02) in $b-y$, 0.00(0.04) in m_1 and 0.00(0.04) in c_1. The data published by Joner & Taylor (1997), with 14 stars in common with our catalogue, up to a limit of $V \sim 13$, give differences of 0.01(0.03) in V, 0.01(0.02) in $b-y$, $-0.02(0.03)$ in m_1 and $-0.01(0.04)$ in c_1. Before Nissen et al. (1987), the study of Strom et al. (1971) with 19 common stars up to a limit of $V \sim 13.5$ gives: $-0.02(0.03)$ in V, $-0.03(0.02)$ in $b-y$, 0.03(0.05) in m_1, $-0.02(0.06)$ in c_1 and $-0.02(0.07)$ in H_β, but a large scatter and a probable colour term in their results was already noted by Nissen et al. (1987).

The V magnitude derived from the y filter can be compared to the published broadband data. Several studies of M 67 give us mean differences in V, in the sense ours minus others (see Table 6.5). With the photoelectric results: $-0.02(\sigma = 0.04)$ $N = 173$ for Eggen & Sandage (1964); 0.01(0.05) $N = 225$ for Sanders (1989). With the CCD photometric results: 0.01(0.03) for the $N = 154$ common stars with the very thorough work by Sandquist (2004); $-0.01(0.05)$ for the $N = 967$ common stars with the most complete study by Montgomery et al. (1993); 0.01(0.06) for the $N = 306$ common with Henden (2003); $-0.01(0.04)$ for the $N = 89$ common with Kim

[3]Table 6.4 is available in electronic form from `Lola.Balaguer@am.ub.es`.

Table 6.5: Comparison of the V magnitude to the published broadband data

Author	$\Delta V_{\mathrm{our-others}}$	σ	N
Eggen & Sandage (1964)	−0.02	0.04	173
Sanders (1989)	0.01	0.05	225
Gilliland et al. (1993)	−0.02	0.03	136
Montgomery et al. (1993)	−0.01	0.05	967
Kim et al. (1996)	−0.01	0.04	89
Henden (2003)	0.01	0.06	306
Sandquist (2004)	0.01	0.03	154

et al. (1996); and −0.02(0.03) for the $N = 136$ common with Gilliland et al. (1993). Looking at the differences, one concludes that there are no systematic trends in our photometry.

6.2 Astrometric Analysis

We have studied the membership segregation using parametric and non-parametric approaches in the same fashion as in Chapters 2 and 4. Thanks to the proper motions obtained by Zhao et al. (1993) from high-quality plates taken with the double astrograph at the Zǒ-Sè station of the Shanghai Observatory, as in the case of NGC 1817 and NGC 2548, we have been able to use the same procedure in a very homogeneous way. Zhao et al. give relative proper motions of 1046 stars within a $1\overset{\circ}{.}5 \times 1\overset{\circ}{.}5$ area in the NGC 2682 region, from PDS measurements of 9 plates. The plates have a maximum epoch difference of 80 years.

The reduction of the relative proper motions was made using the same plate-pair technique adopted many times at Shanghai Observatory and already explained in Chapter 2: all linear and quadratic coordinate-dependent terms and the coma term were included in the plate-pair solution.

The quoted mean errors of proper motions vary from 0.4 mas yr^{-1} for bright stars in the inner part of the cluster field to some 1.5 mas yr^{-1} for faint stars in the

outer part of the cluster. The comparison with the proper motions of Sanders (1977) and Girard et al. (1989) shows a satisfactory agreement. The magnitude limit of Zhao et al.'s study is $V \sim 15.5$.

There are 50 stars in common with the Tycho-2 Catalogue (Høg et al. 2000). From their absolute proper motions we can calculate the transformation of Zhao et al.'s relative proper motions to the absolute reference frame:

$$(\mu_\alpha \cos\delta)_{\rm TYC2} = -6.510\ (\pm 0.259) + 1.013\ (\pm 0.034) \cdot \mu_x - 0.017\ (\pm 1.644) \cdot \mu_y\ ;$$
$$r = 0.956;\ N = 44$$
$$(\mu_\delta)_{\rm TYC2} = -8.051\ (\pm 0.404) + 0.025\ (\pm 0.056) \cdot \mu_x + 0.957\ (\pm 0.056) \cdot \mu_y\ ;$$
$$r = 0.951;\ N = 50$$

where r is the correlation coefficient and proper motions are expressed in mas yr^{-1}.

Membership determination in Zhao et al. (1993) was calculated with an 8-parametric Gaussian model, and a list of stars with probability higher than 0.8 and distance to the centre less than $45'$ gave 282 cluster members. For the sake of coherence with our analysis of NGC 1817 and NGC 2548 (Chapters 2 and 4), we apply a 9-parametric Gaussian model and a non-parametric method to the proper motions obtained by Zhao et al. In contrast to their approach to the segregation of cluster members, we do not use any spatial information, for the same reasons given in previous Chapters.

Zhao et al. give x, y coordinates, proper motions with their errors, number of plates used for proper motion determination, and cross-identifications with Sanders (1977). The authors state that their x, y coordinates are taken from one of the plates, but a detailed analysis of the data shows that this is the case for the majority of the stars, but there is a small subset (61 stars) whose x, y coordinates seem to have been taken from at least two other plates, and this introduces shifts in their quoted positions. Fortunately, Zhao et al.'s cross-identifications with Sanders (1977) were correct, what allowed us a complete cross-identification of our photometric catalogue with the proper motion data not losing any star. This effect in Zhao et al. (1993) x, y data does not affect our results, since we do not use these coordinates in our study. All tests performed show that this effect in Zhao et al.'s data affects only the positions x, y, not the proper motions. The mistake in the x, y coordinates of 61 stars seem to have been introduced in the final preparation of the tables by Zhao et al. (1993).

Table 6.6: Distribution parameters and their uncertainties from a 9-parametric Gaussian model applied to NGC 2682 cluster and the field. The units of μ and σ are mas yr^{-1}

	n_c	μ_x	μ_y	σ_c	σ_{μ_x}	σ_{μ_y}	ρ
NGC 2682	0.364	−0.59	0.49	0.89			
	±0.016	±0.07	±0.06	±0.05			
field		0.02	3.31		9.00	8.63	−0.21
		±0.10	±0.48		±0.03	±0.24	±0.02

6.2.1 The classical approach

The parametric method is calculated with a 9-parametric Gaussian model as thoroughly explained in previous Chapters. The results are shown in Table 6.6. If we transform the mean relative proper motion obtained to the absolute system, we get the mean absolute proper motion for the cluster to be $(\mu_\alpha \cos\delta, \mu_\delta) = (-7.1\pm0.8, -7.6\pm0.4)$ mas yr^{-1}.

Applying Equation (2.11), we obtain a value of the effectiveness of memberbership determination of $E = 0.82$. Such a remarkable effectiveness is what can be expected for a high contrast cluster as M 67.

6.2.2 The non-parametric approach

The cluster/field segregation from astrometry has also been analysed with a non-parametric approach, as explained in Section 2.6.2. The procedure was tested for several subsamples applying different proper motion cutoffs and the adopted one, as in other cases, is of $|\mu| \leq 15$ mas yr^{-1}.

The empirical frequency function determined from the VPD corresponding to the area occupied by the cluster is made up from two contributions: cluster and field. To distinguish the two populations, we studied the VPD for the plate area outside a circle centred on the cluster. We did tests with circles of very different radii (see Figure 6.3 and Table 6.7), searching a reasonable tradeoff between cleanness

and signal-to-noise ratio. The kernel density estimator was applied in the VPD to these data, yielding the empirical frequency function, for a grid with cell size of 0.2 mas yr^{-1}, again well below the proper motion errors.

We finally find that the area outside a circle with a radius of 35′ centred on the cluster yields a clean frequency function with low cluster contamination and low noise. Figure 6.4 displays the empirical PDFs for the mixed population (circle), for the field (outside the circle) and for the cluster (non-field) population. We estimate the typical noise level, γ, present in the result and we restricted the probability calculations to the stars with cluster PDF $\geq 3\gamma$. The maximum of the cluster PDF is located at $(\mu_x, \mu_y) = (-0.6\pm0.2, 0.4\pm0.2)$ mas yr^{-1}, that coincides well with the values obtained in the parametric method. If we transform this value to the absolute system, we get an absolute proper motion for the cluster of $(\mu_\alpha \cos\delta, \mu_\delta) = (-7.1\pm0.7, -7.7\pm0.5)$ mas yr^{-1}. Thirty six out of the 50 Hipparcos stars are classified as members giving a mean value of $(\mu_\alpha \cos\delta, \mu_\delta) = (-8.4\pm2.1, -6.1\pm2.2)$ mas yr^{-1}. This is fully compatible with our result, but we consider our figures more reliable, since they are derived from the whole sample of stars and have a lower uncertainty.

The effectiveness of membership determination for the non-parametric method gives a value of $E = 0.87$. This outstanding value, higher than in the parametric case, emphasises the existence of a well-defined, populated and distinct frequency function for the cluster, with little superposition from the sparse field population of this sky area.

6.2.3 Results and discussion

As already discussed, the non-parametric approach does not take into account the errors of the individual proper motions. But the FWHM of the PDF of the cluster gives an estimation of the width of the distribution. We obtained a FWHM of $\sim$4.1$\pm$0.2 mas yr^{-1}. Taking into account the Gaussian dispersion owed to the smoothing parameter $h = 1.34$ mas yr^{-1}, this would correspond to a r.m.s. error on proper motions of 1.55 mas yr^{-1}. But from Zhao et al. (1993) we know that the mean proper motion precision is 1.24 mas yr^{-1}, what gives us an intrinsic dispersion component of 0.93 mas yr^{-1}, of the same order as the value obtained by the parametric membership determination ($\sigma_c = 0.89\pm0.05$ mas yr^{-1}, ~ 4 km s^{-1} at

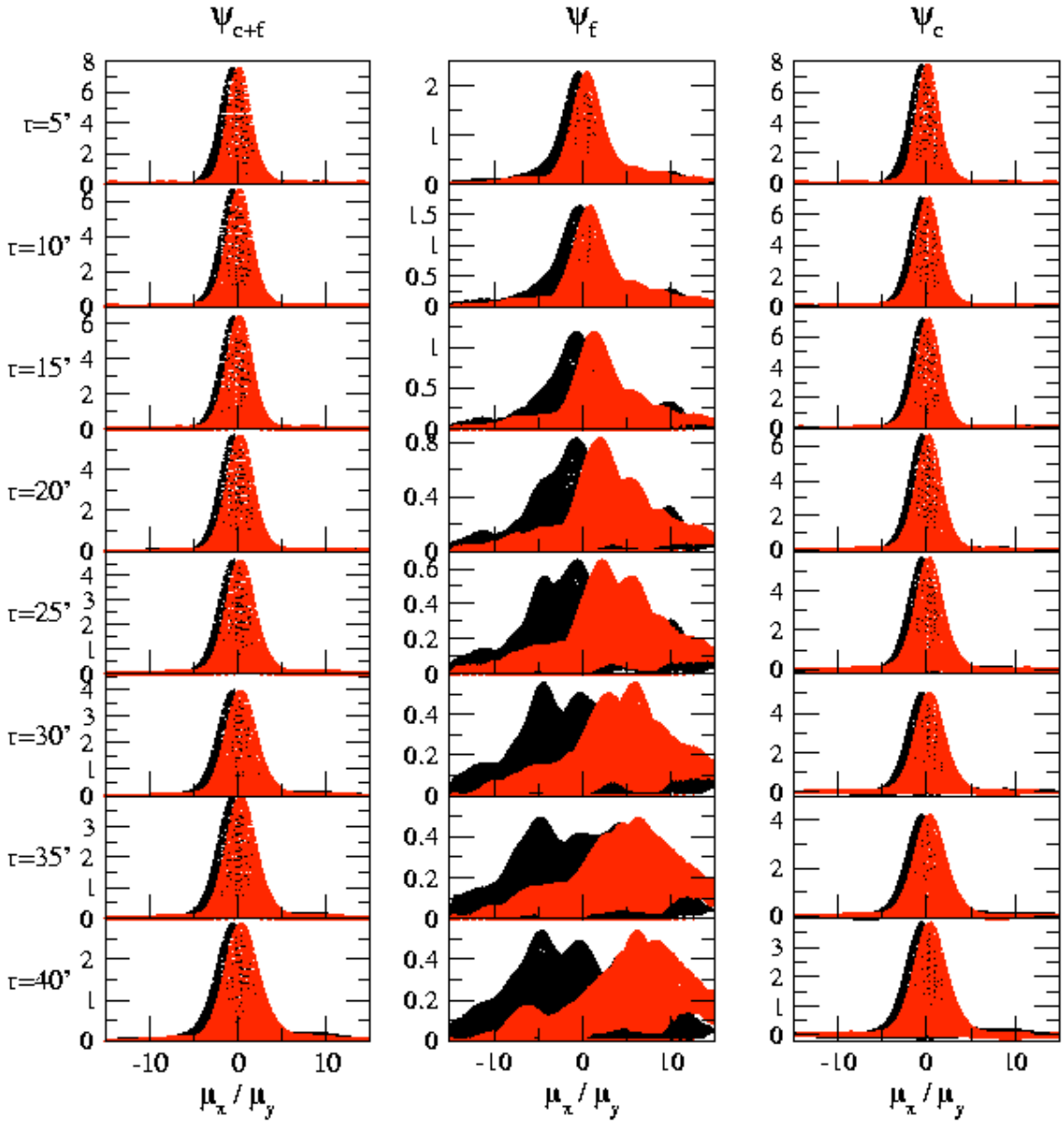

Figure 6.3: Empirical probability density functions of NGC 2682 for the mixed sample, ψ_{c+f}, the field population, ψ_f, and the cluster population, ψ_c, taking different radii for the cluster area, r. At the back μ_x in black, at the front μ_y in red.

Table 6.7: Comparison of the position, maximum and FWHM of the empirical probability density function of the total, the field and the substracted cluster NGC 2682 taking different radii for the cluster area. The last column gives the FWHM for each component (μ_x/μ_y) and the averaged value.

r	$(\mu_x)_{\rm c+f}$	$(\mu_y)_{\rm c+f}$	$(\psi_{\rm c+f})_{\rm max}$	FWHM $_{\psi_{\rm c+f}}$
	$(\mu_x)_{\rm f}$	$(\mu_y)_{\rm f}$	$(\psi_{\rm f})_{\rm max}$	FWHM $_{\psi_{\rm f}}$
	$(\mu_x)_{\rm c}$	$(\mu_y)_{\rm c}$	$(\psi_{\rm c})_{\rm max}$	FWHM $_{\psi_{\rm c}}$
(arcmin)	(mas yr^{-1})	(mas yr^{-1})	-	(mas yr^{-1})
5	-0.6±0.2	0.2±0.2	7.5	3.2/2.8→3.0
	-0.4±0.2	0.6±0.2	2.3	3.8/4.0→3.9
	-0.6±0.2	0.2±0.2	7.8	3.2/2.8→3.0
10	-0.6±0.2	0.2±0.2	6.7	3.2/3.0→3.1
	-0.4±0.2	0.8±0.2	1.6	4.6/4.2→4.4
	-0.6±0.2	0.2±0.2	7.1	3.2/3.0→3.1
15	-0.4±0.2	0.2±0.2	6.4	3.2/3.2→3.2
	-0.6±0.2	1.2±0.2	1.2	5.6/4.8→5.2
	-0.4±0.2	0.2±0.2	7.1	3.2/3.0→3.1
20	-0.4±0.2	0.2±0.2	5.7	3.4/3.2→3.3
	-0.8±0.2	2.0±0.2	0.8	9.6/7.6→8.6
	-0.4±0.2	0.2±0.2	6.6	3.4/3.2→3.3
25	-0.4±0.2	0.2±0.2	4.6	3.8/3.4→3.6
	-0.6±0.2	2.2±0.2	0.6	11.6/9.4→10.5
	-0.4±0.2	0.2±0.2	5.6	3.6/3.4→3.5
30	-0.6±0.2	0.4±0.2	4.0	3.8/3.6→3.7
	-4.4±0.2	6.0±0.2	0.6	14.0/10.2→12.1
	-0.6±0.2	0.4±0.2	5.0	3.8/3.6→3.7
35	-0.6±0.2	0.4±0.2	3.2	4.2/4.0→4.1
	-4.8±0.2	6.4±0.2	0.5	16.2/12.2→14.2
	-0.6±0.2	0.4±0.2	4.2	4.2/4.0→4.1
40	-0.6±0.2	0.4±0.2	2.9	4.2/4.2→4.2
	-4.6±0.2	6.2±0.2	0.5	16.2/14.4→15.3
	-0.6±0.2	0.4±0.2	3.8	4.2/4.0→4.1

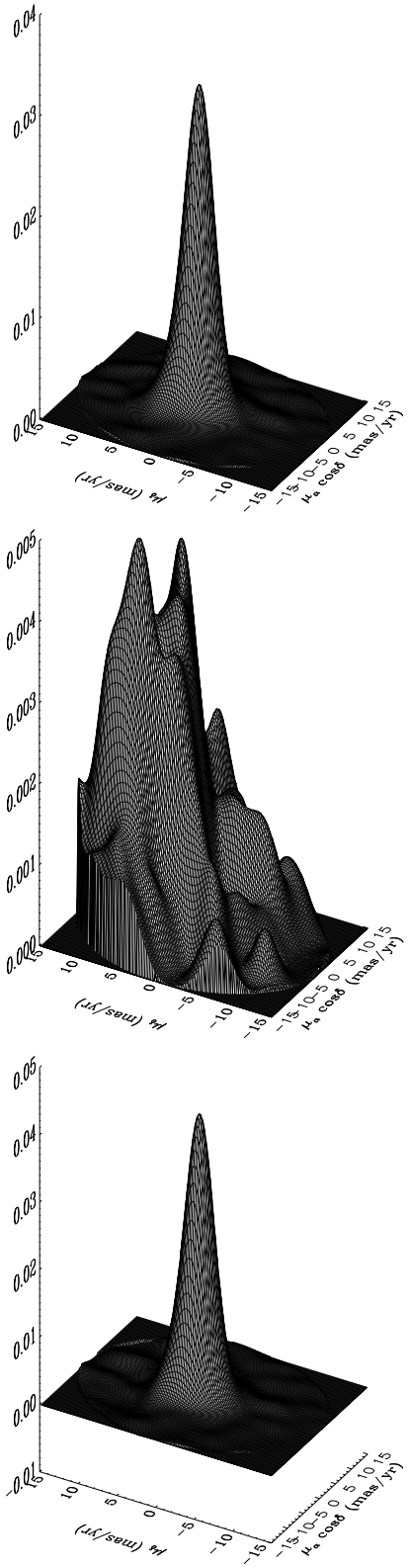

Figure 6.4: Empirical probability density functions in the kinematic plane. Top: ψ_{c+f} mixed sample from the inner circle of 35'. Centre: ψ_f field population from outside this circle. Bottom: ψ_c cluster population of NGC 2682.

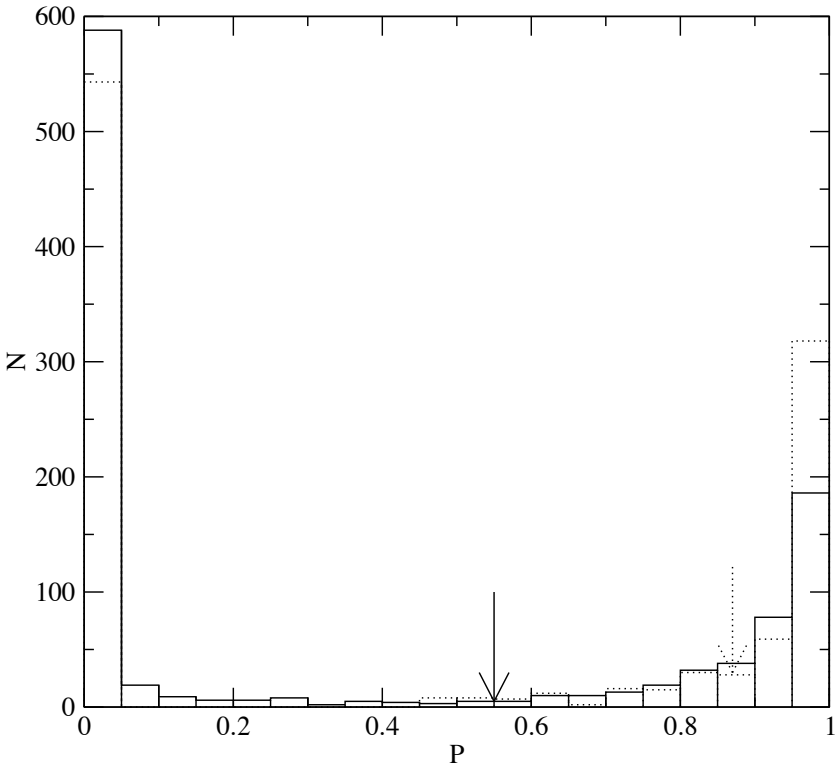

Figure 6.5: The histogram of cluster membership probability of NGC 2682. The solid line gives the results for classical parametric method (Section 6.2.1), while the dotted line corresponds to the non-parametric approach (Section 6.2.2). The arrows mark the limiting probabilities for member selection for each method.

the distance of 900 pc from Section 6.4.1).

The cluster membership probability histogram (Figure 6.5) shows a very clear separation between cluster members and field stars in both approaches (the solid line being the classical parametric method, dotted line the non-parametric approach). The non-parametric approach gives us an expected number of cluster members from the integrated volume of the cluster frequency function in the VPD areas of high cluster density, where PDF$\geq 3\gamma$. The expected amount of cluster members in this VPD area is of 393. Sorting the sample in order of decreasing non-parametric membership probability, P_{NP}, the first 393 stars are the most probable cluster members. The minimum value of the non-parametric probability (for the 393-rd star) is $P_{NP} = 0.87$. Table 6.8[4] lists the cross-identifications with Zhao et al. and Sanders, the P_P and the P_{NP} for the 1046 stars.

[4]Table 6.8 is available in electronic form from `Lola.Balaguer@am.ub.es`.

To decide where to set the limit among members and non-members in the list sorted in order of decreasing parametric membership probability, P_P, we accept the size of the cluster predicted by the non-parametric method, 393 stars. Thus we consider that the 393 stars of highest P_P are the most probable members, according to the results of the parametric technique. The minimum value of the parametric probability (for the 393-rd star) is $P_P = 0.55$. It is worth noting that, contrary to what happened with the previous two clusters and in other cases found in the literature (Galadí-Enríquez et al. 1998a), in this case the original parametric segregation (Zhao et al. 1993) at $P_P > 0.7$ was underestimating, and not overestimating, the number of probable members. This is because M 67 is much more populated than the other clusters.

With these limiting probabilities ($P_{NP} \geq 0.87$; $P_P \geq 0.55$), we get a 97% (1014 stars) of agreement in the segregation yielded by the two methods.

As in previous Chapters, to set up a final and unique list, we accept as probable members those stars classified as member by at least one of the two methods. This way we get a list of 412 astrometric probable member stars.

Figures 6.6 and 6.7 show the proper motion VPD and the sky distribution for all the measured stars, where " $\circ$ " denotes an astrometric probable member of NGC 2682, and all other stars are considered field stars and they are indicated by "+".

A comparison of the cluster/field segregation for the 143 stars in common with the radial velocity study by Mathieu et al. (1986, 1990) is given in Table 6.9. The radial velocities have typical standard deviations for a set of measurements of any given star that range between 0.5 and 0.8 km s^{-1}. To quantify the differences in the segregation, we do as in Section 2.6.4 and set an agreement index P_c to 1 if the parametric probability, P_P, agrees with the radial velocity segregation, 2 if the non-parametric probability, P_{NP}, agrees, 3 if both probabilities, P_P and P_{NP}, agree and 0 if none does. We find 125 out of 143 stars with $P_c > 0$, that is 87% agreement with the radial velocities segregation. 13% of the disagreement consists of 15 stars out of 41 (38%) being considered non-members on the basis of proper motions while only 3 out of 102 (8%) were found to be astrometric members while considered non-members on the basis of radial velocities. Those three have only one measurement of their radial velocities and two of them are known to be SB, therefore the measurement may be different from the systemic velocity and thus they cannot

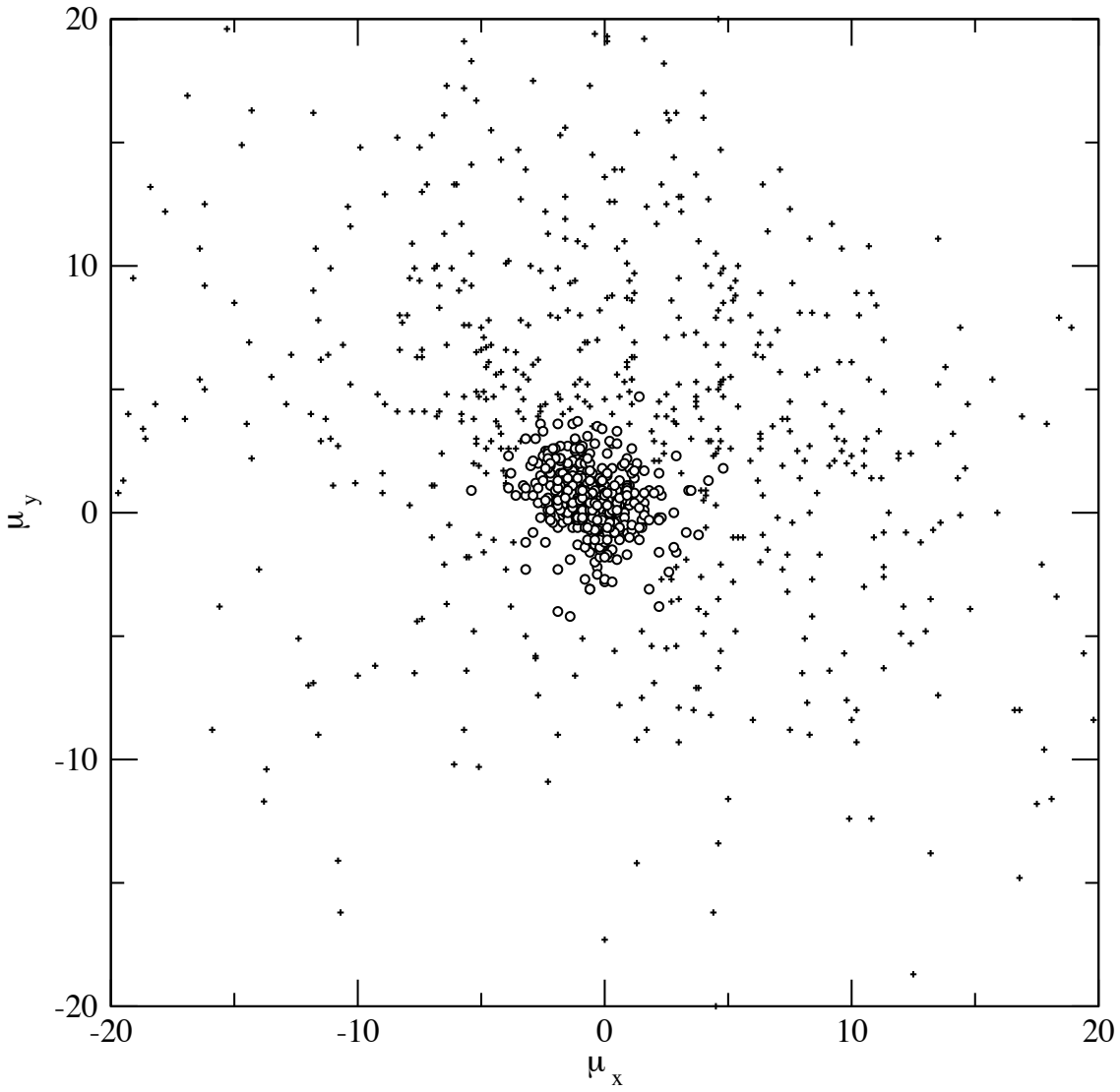

Figure 6.6: The proper motion vector-point diagram of stars in NGC 2682 region. ("○" for the astrometric probable members of NGC 2682 and "+" for field stars). Units are mas yr^{-1}.

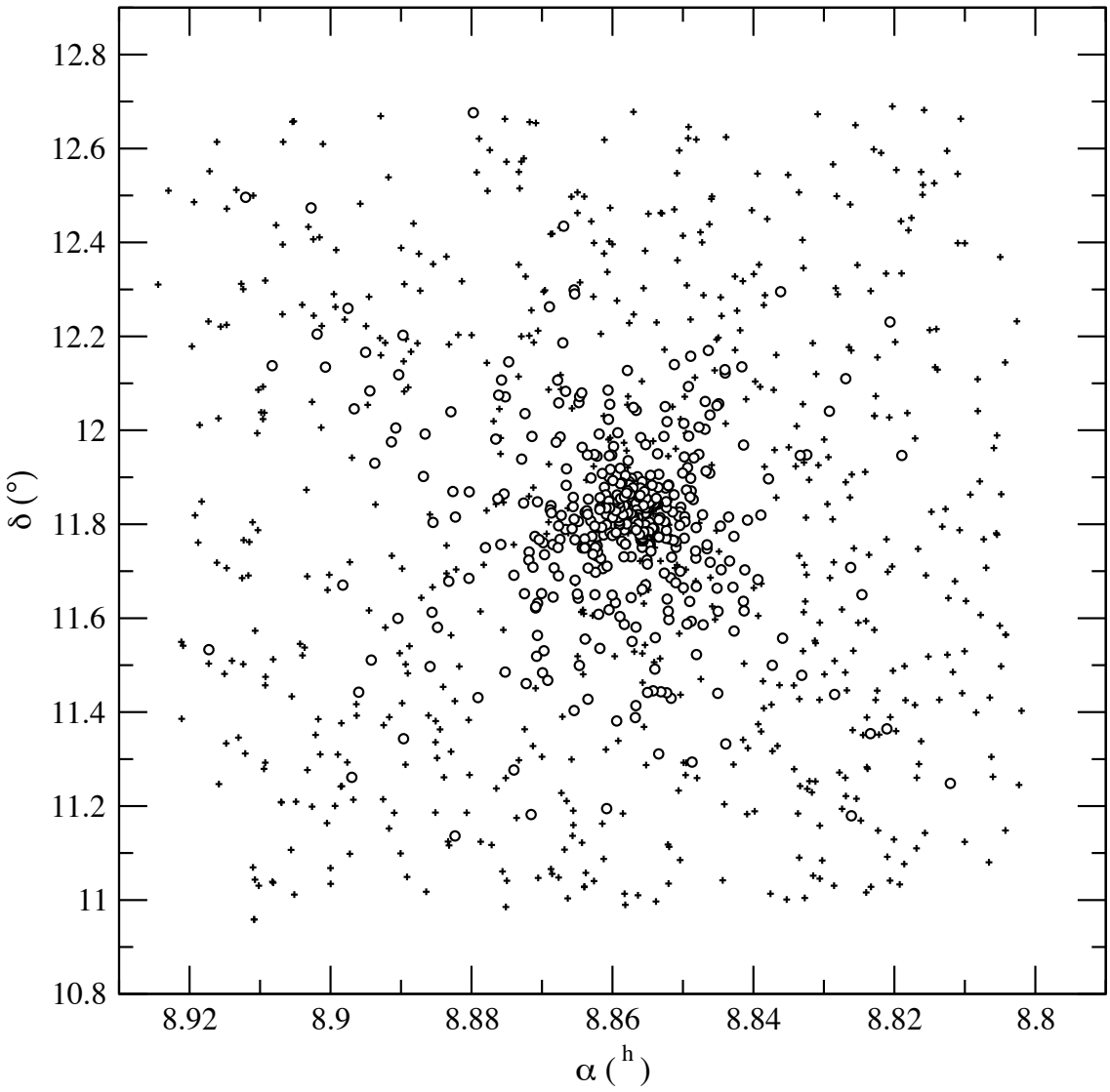

Figure 6.7: The position distribution of stars in NGC 2682 ("○" for the astrometric probable members of NGC 2682 and "+" for field stars)

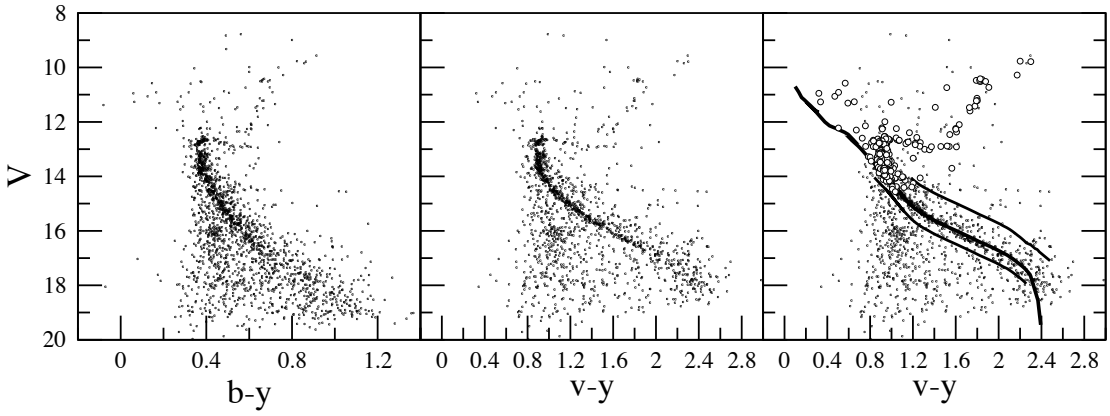

Figure 6.8: The colour-magnitude diagram of the NGC 2682 area. Figure on the right shows the astrometric probable members as empty circles. Thick line is a shifted ZAMS, with the chosen margin for candidate members ($V + 0.5$,$V - 1$) in thin lines. See text for details.

be completely ruled out as members.

If we compare the parametric and non-parametric methods, the behaviour is rather similar. For the parametric method we find a total of 121 stars (85%) whose membership assignation coincides with the radial velocity criterion, while for the non-parametric method this amounts to 124 stars (87%).

6.3 Colour-Magnitude diagrams

We use the V vs $(v - y)$ colour-magnitude diagram for our study because it defines the main-sequence of a cluster significantly better than the traditional V vs $(b - y)$ diagram (Figure 6.8 left and centre). The colour-magnitude diagram of all the stars in the area displays a very well defined main sequence. The advanced age of this cluster is obvious at first sight looking at the diagram. Moreover, the sequence of binaries can be easily followed.

Table 6.9: The cross-identification of stars in common with the radial velocities by Mathieu et al. (1986; 1990) and the comparison of those with the parametric (P_P) and non-parametric (P_{NP}) probabilities. The first part compares the stars considered as members by us, the second part the non-members. See text for explanation of the agreement index P_c.

Id_{BDA}	$Id_{6.8}$	P_P	P_{NP}	P_c	Vr^*	Id_{BDA}	$Id_{6.8}$	P_P	P_{NP}	P_c	Vr^*
4	818	0.94	0.96	3	34.0 ±2.0	16	829	0.88	0.96	3	33.2 ±0.9
18	521	0.92	0.95	3	32.9 ±0.5	20	834	0.96	0.97	3	33.1 ±1.0
22	839	0.95	0.96	3	34.4 ±1.9 SB1	28	840	0.97	0.97	3	33.7 ±1.0
30	845	0.97	0.97	3	33.6 ±0.4	37	846	0.97	0.97	3	33.7 ±0.3
46	843	0.98	0.97	3	33.8 ±0.1	48	848	0.96	0.98	3	33.0 ±0.4
51	849	0.96	0.97	3	34.6 ±0.9	54	863	0.95	0.97	3	34.5 ±0.7
55	862	0.75	0.92	0	42.1 ±0.0 SB	72	876	0.97	0.98	3	33.3 ±0.6
79	860	0.97	0.98	3	34.1 ±1.7	84	966	0.78	0.94	3	34.1 ±0.4
86	933	0.81	0.86	1	27.6 ±0.0	88	927	0.96	0.97	3	34.13±0.23 SB2
95	886	0.98	0.98	3	34.7 ±2.4	96	929	0.96	0.98	3	33.1 ±0.7
101	930	0.97	0.98	3	32.9 ±0.9	102	893	0.98	0.97	3	36.17±0.17 SB1
104	931	0.95	0.97	3	33.5 ±0.4	105	883	0.80	0.94	3	34.3 ±0.7
108	894	0.51	0.93	2	34.7 ±0.6	111	891	0.98	0.97	3	33.70±0.22 SB1
115	918	0.97	0.98	3	34.4 ±0.5	117	887	0.98	0.98	3	34.4 ±0.3 SB2
119	924	0.97	0.97	3	34.34±0.21 SB2	124	912	0.97	0.98	3	29.6 ±0.7 SB
127	911	0.97	0.98	3	33.3 ±0.8	130	910	0.94	0.98	3	33.7 ±0.7
131	972	0.95	0.96	3	33.3 ±2.0 SB2	134	907	0.98	0.97	3	32.5 ±1.2 SB1
135	908	0.97	0.97	3	34.3 ±0.6	136	974	0.94	0.96	3	32.87±0.12 SB1
141	947	0.86	0.95	3	33.6 ±0.4	143	937	0.91	0.96	3	32.93±0.07 SB1
149	949	0.98	0.97	3	35.5 ±0.8	151	971	0.81	0.94	3	33.9 ±0.5
157	976	0.98	0.98	3	33.6 ±0.5	163	995	0.98	0.98	3	33.8 ±0.8
164	983	0.79	0.94	3	33.3 ±0.4	166	4	0.97	0.98	3	33.3 ±0.3
170	953	0.60	0.93	3	33.59±0.10 SB1	174	961	0.97	0.98	3	36.2 ±4.5
176	914	0.97	0.98	3	32.5 ±0.4 SB1	180	985	0.98	0.97	3	35.0 ±0.8
181	955	0.98	0.98	3	33.3 ±0.7	182	956	0.97	0.98	3	32.2 ±2.2
184	987	0.98	0.97	0	61.4 ±0.0	185	958	0.79	0.94	3	33.4 ±0.0
190	989	0.80	0.94	0	43.6 ±0.0 SB	192	603	0.98	0.97	3	32.7 ±1.1
193	999	0.98	0.97	3	33.7 ±0.5	195	1017	0.97	0.98	3	33.87±0.12 SB1
210	1005	0.98	0.97	3	33.9 ±1.1	215	608	0.98	0.98	3	33.6 ±0.6
216	1010	0.97	0.98	3	33.03±0.13 SB1	217	1002	0.97	0.97	3	33.3 ±0.4
218	1006	0.98	0.97	3	34.0 ±0.5	219	1007	0.98	0.98	3	33.4 ±0.3 SB1
223	609	0.68	0.94	3	32.8 ±0.4	224	1011	0.95	0.96	3	32.55±0.07 SB1
226	1013	0.98	0.98	3	32.5 ±1.0	227	1004	0.98	0.97	3	32.8 ±0.7
231	1029	0.97	0.97	3	32.5 ±0.6	236	1025	0.98	0.98	3	33.82±0.18 SB1
237	611	0.97	0.98	3	34.7 ±0.7	238	1028	0.75	0.94	3	38.3 ±0.0
241	1027	0.96	0.96	3	33.2 ±0.7	243	1026	0.96	0.96	3	33.4 ±0.5

(*) Zero errors mean that only one measurement was taken and no dispersion could be calculated.

Table 6.9: Continuation.

244	1032	0.93	0.96	3	33.55±0.05 SB1	248	612	0.98	0.98	3	34.0 ±1.3
252	618	0.97	0.96	3	32.5 ±1.0	255	1043	0.96	0.97	3	31.3 ±0.3
256	226	0.96	0.98	3	33.2 ±0.9	262	1046	0.97	0.97	3	31.6 ±0.7
266	647	0.78	0.94	3	34.3 ±0.4	271	1058	0.93	0.96	3	34.1 ±0.8
272	645	0.97	0.97	3	31.8 ±0.4	281	1060	0.96	0.97	3	33.4 ±0.8
286	697	0.35	0.92	2	33.6 ±0.5	287	698	0.98	0.97	3	32.8 ±0.5
289	683	0.94	0.96	3	32.7 ±0.4	291	700	0.96	0.97	3	34.1 ±0.1
305	133	0.52	0.92	2	34.2 ±0.9	1182	174	0.95	0.98	3	34.6 ±0.9
2079	172	0.98	0.98	3	34.4 ±0.5	2087	211	0.94	0.97	3	31.5 ±3.0
3035	1001	0.98	0.98	3	34.1 ±0.5	3116	642	0.98	0.97	3	33.60±0.13 SB1
4004	939	0.98	0.98	3	33.48±0.19 SB2	4096	578	0.97	0.97	3	34.0 ±0.8
7591	135	0.91	0.96	3	33.4 ±0.8	7657	505	0.28	0.87	2	33.2 ±0.9
8402	231	0.83	0.94	3	33.6 ±0.4	8524	639	0.69	0.89	3	33.6 ±0.7
8571	253	0.94	0.95	3	34.2 ±0.4	8792	282	0.85	0.93	3	33.1 ±0.5
8808	277	0.85	0.94	3	29.6 ±1.0	8832	713	0.97	0.97	3	33.5 ±0.7
Id_{BDA}	$Id_{6.8}$	P_P	P_{NP}	P_c	Vr^*	Id_{BDA}	$Id_{6.8}$	P_P	P_{NP}	P_c	Vr^*
8	822	0.00	0.70	3	29.1 ±1.8	10	136	0.00	0.00	3	16.3 ±0.0
45	857	0.00	0.00	3	-14.0 ±0.0	49	3	0.00	0.00	3	28.1 ±0.0
144	951	0.00	0.00	0	33.72±0.14 SB1	155	943	0.00	0.00	3	3.6 ±1.0
173	963	0.00	0.00	0	33.37±0.20 SB1	200	601	0.00	0.00	3	12.0 ±0.4
206	602	0.00	0.00	0	34.8 ±0.3	240	215	0.17	0.84	3	43.3 ±0.15 SB1
242	1024	0.00	0.00	3	-1.1 ±0.4	277	648	0.00	0.00	3	1.6 ±0.0
2086	210	0.00	0.00	0	33.3 ±0.6	3128	620	0.00	0.00	3	-20.7 ±0.0
4166	481	0.00	0.00	3	-2.5 ±0.0	4168	482	0.00	0.00	3	39.5 ±0.4
7488	485	0.06	0.84	0	33.0 ±0.3	6469	453	0.00	0.00	0	34.1 ±0.2
6470	468	0.00	0.70	0	33.3 ±0.3	6474	495	0.00	0.73	3	9.5 ±0.6
6514	261	0.00	0.00	0	34.5 ±0.7	7112	37	0.00	0.00	3	-9.0 ±0.0
7116	27	0.00	0.00	3	13.7 ±0.0	7232	52	0.00	0.00	3	4.2 ±0.0
7251	434	0.00	0.47	0	34.56±0.14 SB1	7335	75	0.00	0.00	3	-18.9 ±0.0
7350	72	0.00	0.00	3	-13.0 ±0.0	7378	458	0.00	0.00	3	57.8 ±0.0
7434	94	0.00	0.65	0	33.7 ±0.9	7440	98	0.00	0.00	3	14.95±0.11 SB1
7445	85	0.00	0.72	0	33.8 ±1.0	7515	489	0.06	0.84	3	27.6 ±0.6
7551	104	0.00	0.67	3	8.9 ±0.0	7663	492	0.03	0.00	3	1.5 ±0.0
7674	496	0.00	0.00	0	33.7 ±0.5	8135	566	0.00	0.78	0	34.2 ±0.4
8355	623	0.00	0.63	3	49.3 ±0.0	8522	657	0.00	0.00	3	12.6 ±0.0
8533	632	0.00	0.76	3	67.8 ±0.5	8557	250	0.00	0.00	0	33.9 ±0.5
9015	744	0.10	0.81	0	33.5 ±1.6						

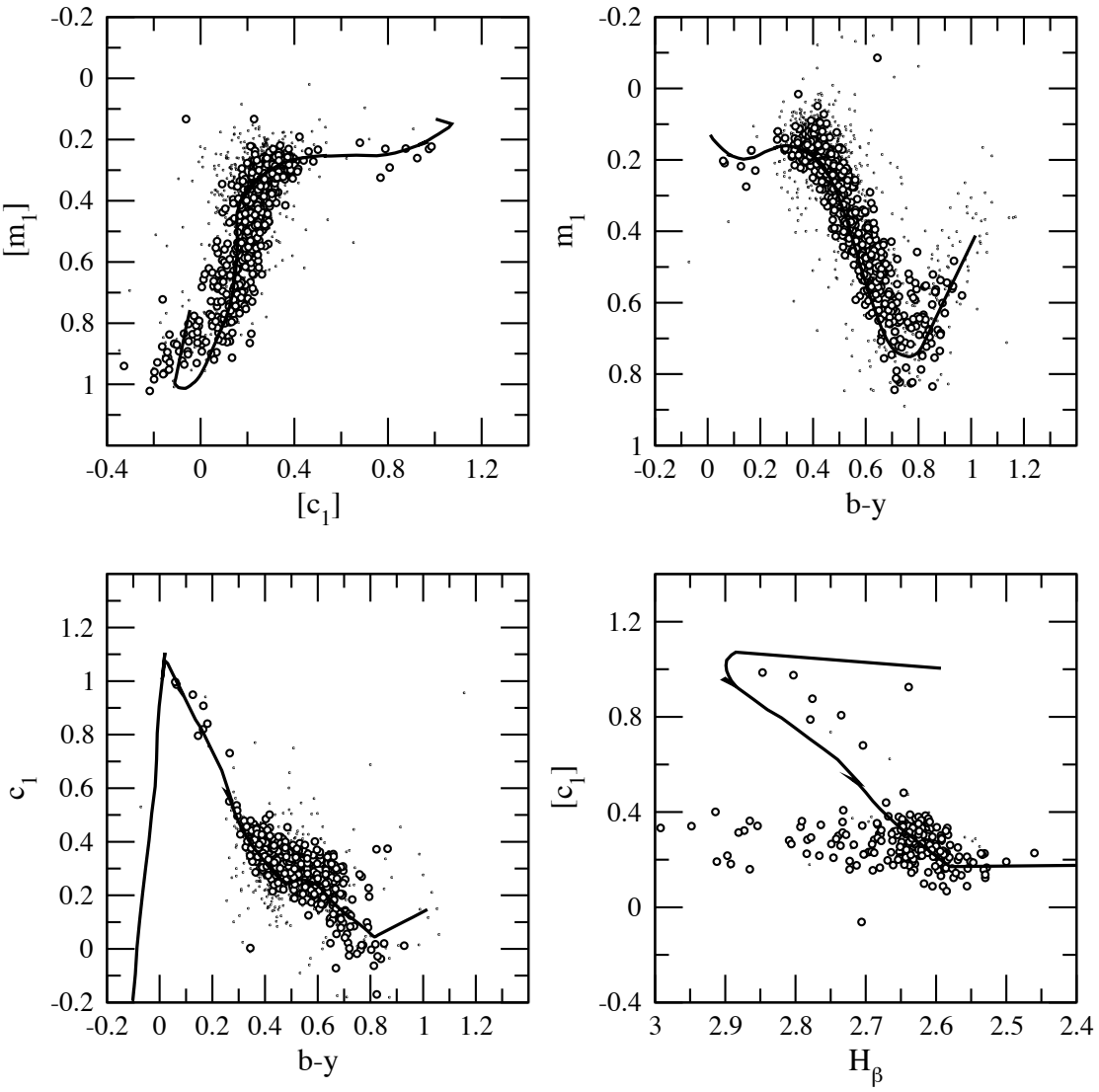

Figure 6.9: The colour-colour diagrams of NGC 2682. Empty circles denote candidate members of NGC 2682, chosen with astrometric and non-astrometric criteria as explained in Section 6.3.1. The thick line is the standard relation shifted $E(b-y) = 0.03$ when necessary. Some of the candidate members, known to be multiple stars, have very discordant values.

6.3.1 Selection of candidate member stars

Our astrometric segregation of member stars has a limiting magnitude of $V \sim 15.5$. From this magnitude down to $V = 18$ we construct a ridge line following a fitting of the observational ZAMS (Crawford 1975, 1978, 1979; Hilditch et al. 1983; Olsen 1984), on the V vs $(v-y)$ diagram. A selection of stars based on the distance to this ridge line is then obtained. The chosen margin for candidates includes all the stars between $V + 0.5$ and $V - 1$ from the ridge line, as shown in the right panel of Figure 6.8.

This first photometric selection is refined in the colour-colour diagrams (Figure 6.9) with the help of the standard relations from the same authors. A final selection of 776 stars in the area are plotted in Figure 6.9 as filled circles in the $[m_1] - [c_1]$, $m_1 - (b-y)$, $c_1 - (b-y)$ and $[c_1] - H_\beta$ diagrams.

6.4 Fundamental parameters of the cluster

Analogously to NGC 1817 and NGC 2548 (Sections 3.3 and 5.3), the stars selected as candidate cluster members were classified into photometric regions and their physical parameters determined, following the algorithm described in Masana (1994) and Jordi et al. (1997). The algorithm uses $uvby - H_\beta$ photometry and standard relations among colour indices for each of the photometric regions of the HR diagram.

6.4.1 Distance, reddening and metallicity

Only 251 stars among the 776 candidate members have H_β measurements. So the computation of physical parameters is only possible for that subset. The results are shown in Figure 6.10. Excluding peculiar stars and those with inconsistence among their photometric indices and computing an average with a 2σ clipping to that subset, we found a reddening value of $E(b-y) = 0.03 \pm 0.03$ (corresponding to $E(B-V) = 0.04$) and a distance modulus of $V_0 - M_V = 9.4 \pm 0.4$ from 136 stars. The distance modulus may be biased towards short values due to the presence of multiple stars treated as if they were single ones. If we divide the clearly separated stars into two groups with higher and lower value than 9.4, we can see from the V

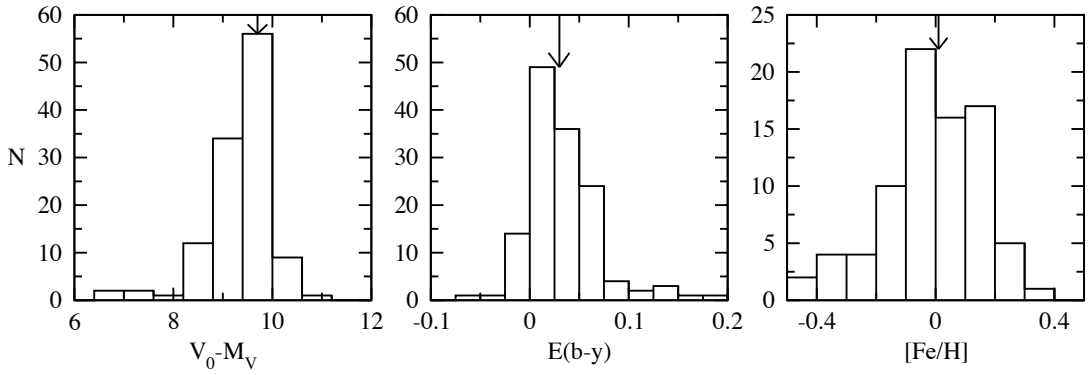

Figure 6.10: The histograms of the distance modulus, reddening and metallicity of the selected member stars of NGC 2682 with H_β measurements. The arrows indicate the mean values adopted for the cluster.

vs $b-y$ diagram that the lower values mainly correspond to stars above the main sequence of the cluster which are most probably multiple stars. Excluding those we can get a value of $V_0 - M_V = 9.7 \pm 0.2$ from the study of 66 stars that very confidently can be considered as singles. Metallicity is better calculated studying only the 81 F and G type stars in our sample following Masana (1994). We find a value of [Fe/H] = 0.01±0.14.

6.4.2 Multiple Star Systems and Blue Stragglers

The high binary content of M 67 was already noted by Racine (1971): "more than half of the M 67 main-sequence stars between G2 and K5 appear to be unresolved multiple stars". Montgomery et al. (1993) studied the distribution of binaries and calculated a 22% of equal-mass component binaries. Trying to account for the binaries with low mass ratios when studying the distribution of multiple stars from a fiducial main sequence, they found a ratio of 38%. Due to the possible presence of very low mass ratio binaries, this percentage is a lower limit. Fan et al. (1996) reconsidered the mass ratios and number of binaries in M 67. And using models leaving the mass ratio to randomly vary from zero to one, they found that the true binary fraction in this cluster depends critically on how to account for the contribution of low mass-ratio binaries. From the models, around a 50% of binaries seems a plausible scenario, with a binary mass ratio distribution more consistent with being random than double-peaked.

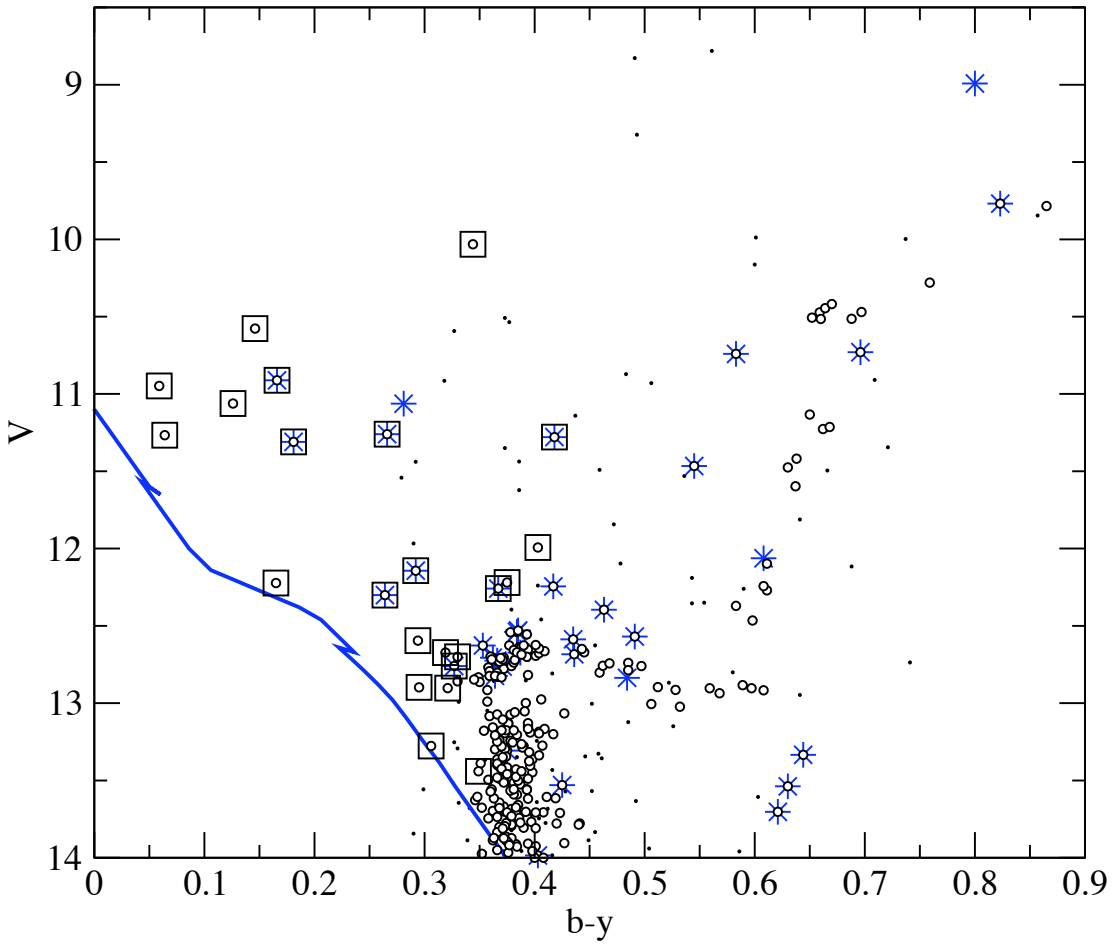

Figure 6.11: Multiple star systems (marked as stars) and blue stragglers (squares) in a colour magnitude diagram of M 67. Circles are candidate member stars. Dots are non-member stars. A ZAMS is shown as reference.

A list of the multiple star systems compiled by Sandquist (2004) and present in our photometry is shown in Table 6.10 with our membership segregation.

The stars S757, S1036, S1282 and ES379, are W UMa contact binaries. W UMa variables are one class of binary star that can produce blue stragglers after angular momentum loss causes the two stars to coalesce.

The blue straggler population of M 67 is believed to be abnormally large with respect to that observed among other open clusters. Ahumada & Lapasset (1995) give a ratio of the number of blue stragglers to that of the main-sequence stars within 2 magnitudes below the turnoff, $N_{\rm BS}/N_2$, of 30/200. But, Deng et al. (1999) based on the photometry by Fan et al. (1996), find that this ratio is 24/286 in much closer agreement with the average found among other open clusters. In our sample we find a similar ratio of $N_{\rm BS}/N_2 = 23/289$. We can conclude that the population of blue stragglers is normal for an intermediate or old cluster. The blue stragglers in our photometry are listed in Table 6.11. Figure 6.11 shows the distribution of multiple star systems and blue stragglers in the colour-magnitude diagram.

The blue stragglers in the colour-magnitude diagram cover the region where the instability strip occurs. Gilliland et al. (1993) discovered two blue stragglers with low amplitude δ Scuti pulsations (S1280 and S1282) and evidence of longer period variations in other stars. Sandquist & Shetrone (2003) discuss that S968, S1066 and S1263 could be long period variables. Sandquist et al. (2003) and van den Berg et al. (2001) point that S1082 is probably a RS CVn star, a close binary and also X-ray source. S1082 may be part of a triple system with two components being blue stragglers and whose brightest component shows some evidence of being a δ Scuti star. Other blue stragglers detected in X-rays, S997 and S1072, have wide eccentric orbits whose nature is still not understood (van den Berg et al. 2004). Also with an eccentric orbit, S1284 is an X-ray source, too. We will come back to these data in the analysis of Section 7.8.

6.4.3 Age

The recent publication by Clem et al. (2004) of empirically constrained colour-temperature relations in the Strömgren system makes possible an isochrone fitting to our results. The best fitting is found for the Pietrinferni et al. (2004) tracks.

Table 6.10: The cross-identification of known multiple star systems and their astrometric segregation (last column). First column is our identification number (Table 6.3), second column that from BDA and third that from Sanders (1977).

$Id_{6.3}$	Id_{BDA}	Id_S	$b-y$	V	m_1	c_1	H_β	M/NM
609	22	821	0.371±0.001	12.764±0.003	0.150±0.002	0.436±0.003		M
629	24	760	0.375±0.001	13.307±0.003	0.180±0.002	0.418±0.004	2.683±0.041	M
761	55	752	0.181±0.001	11.310±0.003	0.230±0.002	0.841±0.004	2.735±0.006	M
777	61	757	0.425±0.004	13.530±0.003	0.124±0.006	0.410±0.008	2.640±0.000	M
806	65	1077	0.435±0.002	12.587±0.003	0.173±0.003	0.358±0.004	2.638±0.005	
905	86	1063	0.630±0.001	13.538±0.003	0.377±0.002	0.244±0.004	2.575±0.008	M
910	88	1053	0.417±0.001	12.245±0.003	0.211±0.002	0.375±0.004	2.605±0.008	M
924	90	975	0.281±0.001	11.063±0.003	0.166±0.002	0.676±0.004	2.666±0.011	NM
962	102	2206	0.463±0.001	12.396±0.003	0.241±0.002	0.346±0.004	2.607±0.014	M
992	111	986	0.366±0.001	12.725±0.003	0.177±0.002	0.414±0.003	2.624±0.010	M
1005	117	999	0.491±0.001	12.569±0.003	0.254±0.002	0.308±0.003	2.595±0.003	M
1015	119	1045	0.384±0.001	12.539±0.003	0.165±0.002	0.393±0.003	2.621±0.004	M
1029	123	1070	0.403±0.004	13.985±0.003	0.167±0.004	0.343±0.005	2.601±0.012	M
1033	124	997	0.292±0.001	12.143±0.003	0.172±0.002	0.536±0.004	2.646±0.005	M
1046	131	1082	0.266±0.003	11.260±0.003	0.120±0.006	0.731±0.008	2.704±0.007	M
1050	134	984	0.367±0.001	12.259±0.003	0.180±0.002	0.409±0.004	2.626±0.000	M
1060	136	1072	0.418±0.001	11.279±0.003	0.160±0.002	0.452±0.004	2.629±0.007	M
1101	143	1040	0.545±0.001	11.466±0.003	0.319±0.002	0.330±0.003	2.531±0.037	M
1102	144	1000	0.484±0.001	12.836±0.003	0.253±0.002	0.364±0.004	2.596±0.002	NM
1176	161	1036	0.327±0.004	12.760±0.004	0.159±0.005	0.380±0.008	2.660±0.006	M
1206	170	1250	0.823±0.012	9.769±0.009	0.555±0.012	0.372±0.009	2.593±0.009	M
1223	173	1264	0.608±0.001	12.063±0.003	0.428±0.002	0.337±0.004	2.589±0.012	NM
1237	176	1234	0.353±0.002	12.627±0.003	0.165±0.021	0.393±0.046	2.626±0.008	M
1300	190	1284	0.166±0.002	10.912±0.003	0.173±0.003	0.908±0.004	2.776±0.003	M
1324	195	1242	0.436±0.002	12.684±0.003	0.197±0.003	0.362±0.004	2.632±0.025	M
1352	205	1282	0.644±0.028	13.334±0.010	-0.086±0.030	0.350±0.028	2.460±0.028	M
1351	207	1195	0.264±0.001	12.301±0.003	0.143±0.003	0.551±0.004		M
1402	216	1216	0.387±0.004	12.673±0.004	0.136±0.004	0.379±0.004	2.728±0.056	M
1412	219	1272	0.385±0.001	12.530±0.003	0.163±0.002	0.380±0.004	2.679±0.075	M
1428	224	1221	0.696±0.001	10.730±0.003	0.517±0.003	0.308±0.004	2.713±0.005	M
1488	244	1237	0.583±0.002	10.741±0.003	0.350±0.003	0.350±0.005		M
987	1050	972	0.556±0.003	15.395±0.004	0.277±0.004	0.238±0.007	2.593±0.004	
1150	3079	ES379	0.668±0.003	15.788±0.003	0.430±0.005	0.139±0.008		
1567	3116	1508	0.364±0.005	12.823±0.004	0.185±0.006	0.386±0.007		M
1085	4004	1024	0.362±0.001	12.706±0.003	0.170±0.002	0.373±0.003	2.624±0.001	M
1126	5808	1113	0.621±0.001	13.703±0.003	0.321±0.003	0.188±0.006		M
1095	5748	1019	0.513±0.001	14.338±0.003	0.283±0.002	0.241±0.004	2.572±0.015	M
277	7440	440	0.800±0.002	8.992±0.003	-0.062±0.003	0.688±0.004		NM

Table 6.11: The cross-identification of blue stragglers and their astrometric segregation (last column). First column is our identification number (Table 6.3), second column that from BDA, and third that from Sanders (1977).

$Id_{6.3}$	Id_{BDA}	Id_S	$b-y$	V	m_1	c_1	H_β	M/NM
559	16	751	0.330±0.001	12.700±0.003	0.172±0.002	0.464± 0.004	2.914±0.029	M
761	55	752	0.181±0.001	11.310±0.003	0.230±0.002	0.841± 0.004	2.735±0.006	M
883	81	977	0.344±0.004	10.032±0.003	0.016±0.005	0.003± 0.026	2.706±0.005	
947	95	1005	0.319±0.001	12.673±0.003	0.191±0.002	0.450± 0.003	2.637±0.006	M
1033	124	997	0.292±0.001	12.143±0.003	0.172±0.002	0.536± 0.004	2.646±0.005	M
1042	130	2204	0.295±0.001	12.898±0.003	0.168±0.002	0.496± 0.004	2.671±0.004	M
1046	131	1082	0.266±0.003	11.260±0.003	0.120±0.006	0.731± 0.008	2.704±0.007	M
1050	134	984	0.367±0.001	12.259±0.003	0.180±0.002	0.409± 0.004	2.626±0.000	M
1060	136	1072	0.418±0.001	11.279±0.003	0.160±0.002	0.452± 0.004	2.629±0.007	M
1140	153	968	0.064±0.001	11.267±0.003	0.209±0.002	0.987± 0.004	2.803±0.008	M
1154	156	1066	0.059±0.001	10.948±0.003	0.203±0.003	0.997± 0.004	2.847±0.003	M
1176	161	1036	0.327±0.004	12.760±0.004	0.159±0.005	0.380± 0.008	2.660±0.006	M
1272	184	1280	0.165±0.001	12.223±0.003	0.174±0.002	0.820± 0.004	2.779±0.011	M
1274	185	1263	0.126±0.001	11.062±0.003	0.218±0.002	0.949± 0.004	2.639±0.012	M
1300	190	1284	0.166±0.002	10.912±0.003	0.173±0.003	0.908± 0.004	2.776±0.003	M
1351	207	1195	0.264±0.001	12.301±0.003	0.143±0.003	0.551± 0.004		M
1370	210	1273	0.375±0.001	12.220±0.003	0.160±0.002	0.403± 0.003	2.641±0.011	M
1649	282	1440	0.349±0.005	13.441±0.005	0.112±0.007	0.442± 0.007		M
1087	4006	1031	0.306±0.001	13.277±0.003	0.171±0.002	0.428± 0.003	2.648±0.008	M
1181	9226	2226	0.294±0.004	12.596±0.004	0.139±0.005	0.517± 0.006		
1529	261	1466	0.146±0.002	10.577±0.003	0.275±0.003	0.796± 0.004		M
261	7489	489	0.321±0.002	12.903±0.003	0.187±0.003	0.478± 0.004		M
659	30	792	0.403±0.002	11.993±0.003	0.132±0.003	0.485± 0.004	2.732±0.014	M

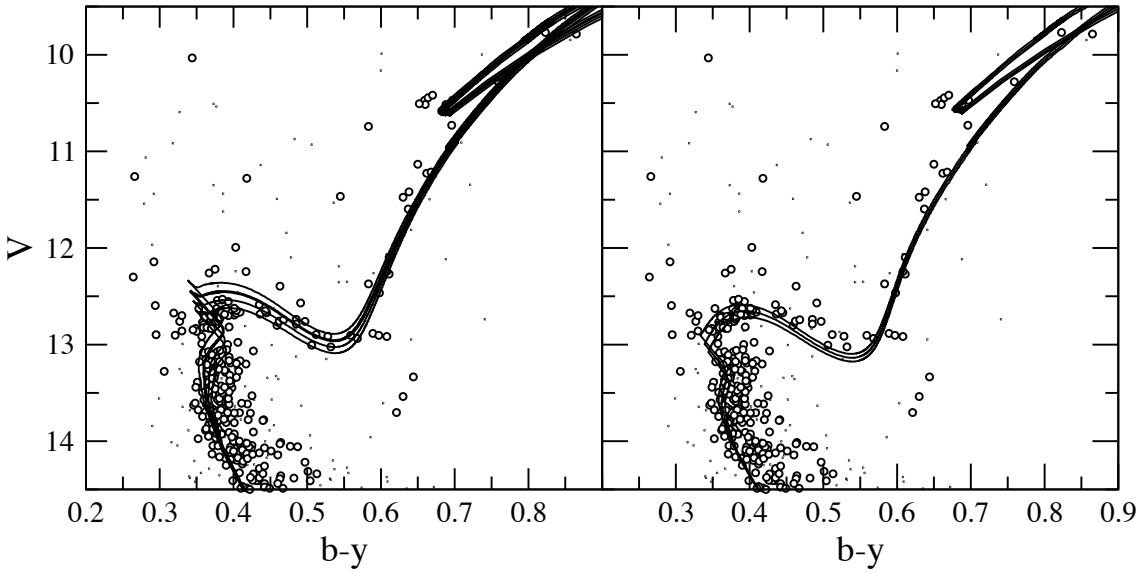

Figure 6.12: Isochrones from Pietrinferni et al. (2004) for scaled solar models of solar metallicity and ages of of 4.0, 4.2, 4.4 and 4.6 Gyr for models with overshooting (left panel) and ages of 3.4, 3.6, 3.8 Gyr for canonical models (right panel). Empty circles are candidate members. The addopted reddening and distance modulus are $E(b-y) = 0.03$ and $V_0 - M_V = 9.7$.

Figure 6.12 shows isochrones of $Z = 0.0198$ shifted by a reddening $E(b-y) = 0.03$ and a distance modulus of $V_0 - M_V = 9.7$ (871 pc) for canonical models (right panel) and models with overshooting (left panel). The best fit is found for an age of 4.4 Gyr in the overshooting model or 3.8 Gyr in the canonical one, very close to the result obtained by Pietrinferni et al. from broadband photometry. A detailed discussion about the amount of overshooting necessary can be found in VandenBerg & Stetson (2004), among others. We adopt an age of 4.2±0.4 Gyr, in agreement with previous estimates.

6.4.4 Dimension and mass

Studying the astrometric selection we found a half-sample radius of $r_{\rm h} = 9.84'$. Taking the calculated distance of 0.9 kpc, it means a half-sample radius of 2.6 pc. The total stellar density was taken in the same way as in previous Chapters from the central density of the cluster, inside the half-sample radius, but taking into account the photometric selection. The stellar density is of $\sigma = 3.61$ stars pc^{-3} and a corresponding mean space density is $\rho = 3.86$ M$_\odot$ pc^{-3}.

We can calculate the total mass of the cluster from the 776 candidate members in Section 6.3.1. Without considering the binaries, we obtain a result of 800 $M_\odot$ as a lower limit.

6.4.5 Comparison with other studies

The fundamental parameters of NGC 2682 are resumed in Table 6.12. Our results are consistent with previous studies. From colour-colour plots in $UBVI$ CCD photometry of 1468 stars within $15'$ of the centre and a limiting magnitude $V = 20$, Montgomery et al. (1993) derived a reddening of $E(B-V) = 0.05\pm0.01$, a metallicity of [Fe/H] $= -0.05\pm0.03$, and from cluster fitting to theoretical isochrones, derived a $V_0 - M_V = 9.45$ and an age between 3 and 5 Gyr. From that photometry, Dinescu et al. (1995) compared several sets of isochrones and they found an age of 4.0 ± 0.5 Gyr, asumming solar metallicity. Carraro et al. (1996) using their own set of theoretical models yielded a distance modulus of $V_0 - M_V = 9.57$ and $E(B-V) = 0.025$, $Y = 0.275$, $Z = 0.018$ and an age of 4 Gyr. Sandquist (2004) gives $V_0 - M_V = 9.60\pm0.03$ assuming $E(B-V) = 0.04\pm0.01$ and [Fe/H] $= 0.02\pm0.06$ from an extensive set of BVI observations. From $V-K$ main-sequence fitting, Sarajedini et al. (2004) found a distance modulus of $V_0 - M_V = 9.62\pm0.07$, assuming solar metallicity and $E(B-V) = 0.04\pm0.01$. The determination of ages of Salaris et al. (2004) give an age of 4.30 ± 0.50 Gyr with a [Fe/H] $= 0.02\pm0.06$ and a distance of 905 pc, in very good agreement with our results, as already happened for NGC 1817 in Chapter 3.3.2.

Fan et al. (1996) studying an area of $1.^\circ92 \times 1.^\circ92$ give a total mass of 1016 $M_\odot$ without binary correction and 1270 $M_\odot$ taking binaries into account. Montgomery et al. (1993) give a present-day mass of 724 $M_\odot$ in a much smaller area, and Francic (1989) gives a lower limit of 553 $M_\odot$ while McNamara & Sanders (1978) give a mass of 1100 $M_\odot$. Therefore, our value of 800 $M_\odot$ is well within the values quoted by other authors.

Table 6.12: Fundamental parameters of NGC 2682

Identifiers	NGC 2682, M 67, C 0847+120, OCl 549.0
Position	$\alpha_{2000} = 8^{\rm h}51^{\rm m}.3$, $\delta_{2000} = +11°50'$
	$l = 215°.66$, $b = +31°.91$
	in Cancer
Distance	$V_0 - M_V = 9.7 \pm 0.2$
	$d = 900$ pc
	$z = 476$ pc
Half-sample radius	$r_{\rm h} = 9.84'$ (2.6 pc)
Proper motion	$\mu_\alpha \cos\delta = -7.1 \pm 0.8$ mas yr^{-1}
	$\mu_\delta = -7.6 \pm 0.4$ mas yr^{-1}
Reddening	$E(b-y) = 0.03 \pm 0.03$
	$E(B-V) = 0.04 \pm 0.04$
Age	$\log t = 9.62 \pm 0.02$
	$t = 4.2 \pm 0.2$ Gyr
Metallicity	[Fe/H] $= +0.01 \pm 0.14$
Membership	N(M) = 412 ($V_{\rm lim}$=14.5) in an area of $1°.6 \times 1°.6$
	N(M) = 776 ($V_{\rm lim}$=18) in an area of $50' \times 50'$
Giants	N(RG) = 46
(in an area of $50' \times 50'$)	N(RG-SB) = 9
Blue Stragglers	N(BS) = 23
	N(BS-SB) = 8
Central stellar density	$\sigma = 3.61$ stars pc^{-3}
	$\rho = 3.86$ M$_\odot$ pc^{-3}
Cluster Mass	$M_{\rm tot} > 800$ M$_\odot$